Cell

Resource

Probing Nucleosome Function: A Highly Versatile Library of Synthetic Histone H3 and H4 Mutants

Junbiao Dai,[1,3] Edel M. Hyland,[1,3] Daniel S. Yuan,[1] Hailiang Huang,[1,2] Joel S. Bader,[1,2] and Jef D. Boeke[1,*]
[1]High Throughput Biology Center, Johns Hopkins University School of Medicine, Baltimore, MD 21205, USA
[2]Department of Biomedical Engineering, Johns Hopkins University, Baltimore, MD 21218, USA
[3]These authors contributed equally to this work
*Correspondence: jboeke@jhmi.edu
DOI 10.1016/j.cell.2008.07.019

SUMMARY

Nucleosome structural integrity underlies the regulation of DNA metabolism and transcription. Using a synthetic approach, a versatile library of 486 systematic histone H3 and H4 substitution and deletion mutants that probes the contribution of each residue to nucleosome function was generated in *Saccharomyces cerevisiae*. We probed fitness contributions of each residue to perturbations of chromosome integrity and transcription, mapping global patterns of chemical sensitivities and requirements for transcriptional silencing onto the nucleosome surface. Each histone mutant was tagged with unique molecular barcodes, facilitating identification of histone mutant pools through barcode amplification, labeling, and TAG microarray hybridization. Barcodes were used to score complex phenotypes such as competitive fitness in a chemostat, DNA repair proficiency, and synthetic genetic interactions, revealing new functions for distinct histone residues and new interdependencies among nucleosome components and their modifiers.

INTRODUCTION

The core histones H3, H4, H2A, and H2B, comprising the fundamental unit of DNA compaction, are among the most highly conserved eukaryotic proteins. Maintenance of specific chromatin structure/state(s) across phyla may underlie this conservation. Indeed, key residues play vital roles in nucleosome assembly (Schwartz and Ahmad, 2006; Ye et al., 2005). Recent studies have highlighted the roles of specific residues, and segments of the unstructured histone tails, to higher-order chromatin structure (Altaf et al., 2007; Fingerman et al., 2007; Jenuwein and Allis, 2001; Shogren-Knaak et al., 2006). Also, studies implicate core histones in nuclear processes independent of their role as a mere DNA scaffold, illustrating that histones are highly dynamic, multifunctional proteins (Ozdemir et al., 2006; Park et al., 2002).

One mechanism by which histones accommodate a range of functions is through posttranslational modification of particular side chains within their amino acid sequence. Lysine (K) and arginine (R) methylation, serine (S) and threonine (T) phosphorylation, lysine acetylation, ubiquitylation, and sumoylation have all been detected on yeast core histone proteins, and most of these alterations are reversible (Klose and Zhang, 2007; Kouzarides, 2007). The N-terminal flexible "tail" domains of histones are the most heavily modified portions, but modifications have also been detected within the globular core (Masumoto et al., 2005; Xu et al., 2005; Ye et al., 2005; Ng et al., 2002; van Leeuwen et al., 2002). This dynamic alteration of nucleosome composition underlies the ability of histones to carry out specific roles, either directly or indirectly through the recruitment of accessory factors, highlighting the mechanistic significance of modifiable histone residues within the nucleosome. Additionally, growing evidence suggests that cellular processes may be regulated redundantly or cooperatively by multiple modifications. For example histone H4 tail acetylation and histone H3K4 trimethylation are both intimately associated with transcription initiation (Berger, 2007; Morillon et al., 2005) while the repair of double-strand breaks requires both H4 S1 phosphorylation and H3 K79 methylation (Cheung et al., 2005; Utley et al., 2005; Zhou et al., 2006), indicating that combinations of modifications on histone residues contribute to a given cellular process.

Not all functions of histone proteins can be attributed to modification state and indeed, nucleosome mutational analyses have revealed both individual residues and unique clusters of amino acids that contribute to DNA-damage response, transcriptional activation, or heterochromatin formation (Hyland et al., 2005; Matsubara et al., 2007). Additionally histone residues can directly interact with proteins such as Isw1p (Zhou et al., 2006), Asf1p (Adkins et al., 2007; Natsume et al., 2007), Dot1p (Fingerman et al., 2007), and Sir3p (Onishi et al., 2007). Prior mutational analyses of histone structure-function were limited to defined subsets of residues, e.g., modifiable residues (Hyland et al., 2005), surface residues (Matsubara et al., 2007), or mutations selected based on a defined cellular process. They relied on laborious analyses of individual strains, hindering scale up of conditions tested. We therefore sought to generate a tool to probe the importance of every nucleosome residue that could be exploited efficiently with many experimental approaches, ultimately elucidating contributions of all residues to nucleosome function.

Here we report the generation of a systematic library of histone H3 and H4 mutants consisting of 486 alleles. We systematically

substituted each residue with alanine and changed all alanine residues to serine. We exploited the physical characteristics of relevant side chains by eliminating charge or reversing size. To investigate the influence of modification states, when possible we substituted all modifiable residues with amino acids mimicking modified and unmodified states. Proline residues were changed to valine, to eliminate proline isomerization, which affects transcription (Nelson et al., 2006). Additionally we probed the histone tails by including 79 systematic N-terminal deletions. Each mutant is linked to two unique 20 bp TAG sequences ("barcodes"), allowing for microarray-based analysis of the library for quantitative or otherwise labor-intensive phenotypic assays.

We screened the library for individual mutants impairing response to the DNA-damaging agents camptothecin (CPT), methyl-methanesulfonate (MMS), hydroxyurea (HU), or UV radiation. We also screened for sensitivity to 6-azauracil (6AU) or benomyl, which perturb the transcription cycle and microtubules, respectively. We determined whether transcriptional silencing at all three silent loci was compromised by histone alleles, providing an insight into heterochromatin structure (Supplemental Experimental Procedures available online).

We also examined several complex phenotypes that are more labor intensive. One of these probed evolutionary fitness in adaptation to glucose-limited medium. We examined proficiency at nonhomologous end-joining (NHEJ). Finally we describe a variation on SLAM (synthetic *l*ethality *a*nalyzed by *m*icroarray) (Ooi et al., 2003) in which a chromosomal null allele of interest is combined with each H3 and H4 mutant to uncover genetic interactions between specific histone residues and potential *trans*-acting factors.

RESULTS

Design of a Versatile Episomal/Integratable Synthetic Histone Cassette

To develop a maximally useful and flexible resource, we designed a synthetic cassette with unique features allowing (1) use of a wide range of selectable markers, (2) delivery either as a replication-competent episome or integrated at a native histone locus with high fidelity, and (3) use in complex phenotype analyses too labor intensive for individual mutants (overall design; Figure 1A).

There are two selectable markers in the construct, *TRP1* and *URA3*. *TRP1* is designed for use in introducing the mutations as part of a CEN (episomal single copy) vector (Figure 1A). *URA3* and flanking DNA segments *HHT2L* and *HHF2R* are used to integrate the cassette at *HHT2-HHF2* (replacing one of two loci at which H3/H4 genes normally reside; Figure 1B). *URA3* is itself flanked by *loxP* sites, facilitating *URA3* removal in *E. coli* or yeast (Sauer, 1987) or replacement of *URA3* by any other *loxP*-flanked selectable marker (Güldener et al., 2002). This design allows one mutant library to be used in a wide variety of genetic contexts.

To be useful for targeted integration, efficient targeting of the resident *HHT2-HHF2* locus and replacement with the mutant copy on the plasmid are needed, and gene targeting was precise (Supplemental Experimental Procedures). Tests of simple phenotypes can be scaled up and performed in the traditional manner on the surface of agar plates by replicating devices. However some phenotypes are more complex and/or require plating on a series of different media before phenotypic scoring. Molecular barcodes or TAGs have been used for such applications and to study genetic interactions. Pairs of TAGs were assigned to each mutant; a subset of the ~12,000 molecular barcodes used in the yeast knockout collection (Winzeler et al., 1999) was used to tag the mutants (Experimental Procedures).

Library of Histone H3 and H4 Mutants

Gene synthesis was employed to create a library of 486 barcoded histone H3 and H4 mutants containing a number of systematic amino acid substitutions (Supplemental Experimental Procedures; Figure 1C). For example, in addition to a complete alanine scan, all lysine residues were additionally mutated to arginine and glutamine to potentially mimic constitutively deacetylated/acetylated states. The collection also contains sets of 52 and 27 systematic deletion alleles of the N termini of H3 and H4, respectively, ranging in size from 4 to 36 residue deletions. These deletion series extend from the N termini to residues H3 36 and H4 24, the positions at which the tails emerge from the nucleosome core; endpoints are placed every 4 residues; deletions made and studied previously by other investigators were added.

All 486 mutations were integrated at *HHT2-HHF2* in two distinct strain backgrounds, GRF167 and S288C, in the presence of wild-type (WT) histone proteins encoded by shuffle plasmid pJP11; viable mutants were also banked after shuffling.

Histone Mutation Database

A histone mutation database documenting the validated phenotypes of all mutants described here and in other systematic mutagenesis studies (Hyland et al., 2005; Matsubara et al., 2007; Park et al., 2002) was established that allows searching by residue, phenotypes, and other parameters. It displays phenotypic data, performs clustering and other analyses, and allows visualization. It was essential for interpreting comprehensive screens. The database, available at http://www.histonehits.org, will be described in detail elsewhere (H.H., E.M.H., J.D., A. Norris, P. Lee, J.D.B. and J.S.B., unpublished data).

Complex Lethality Profiles of H3 and H4 Mutants

The ability of each mutant to survive in the absence of WT was initially determined by a plasmid shuffle technique. Mutants were denoted lethal if integrated copies failed to produce plasmid-free segregants after extended subculturing on nonselective medium. In total, 47 of 407 point mutants, encompassing 40 residues, failed to support viability in both strain backgrounds (Figure 2A). It is remarkable how many residues in these highly conserved proteins can be mutated and retain basic nucleosomal function.

Mapping the residues affected by lethal substitution mutations to the nucleosome structure revealed two nucleosome surface locations highly sensitive to amino acid changes, the nucleosome entry/exit site and the nucleosome dyad axis (Figure 2A). The surface residues required for viability were largely restricted to those interacting directly with DNA (Figure 2B). A second set of lethal mutants was in the hydrophobic core. Nearly all of these

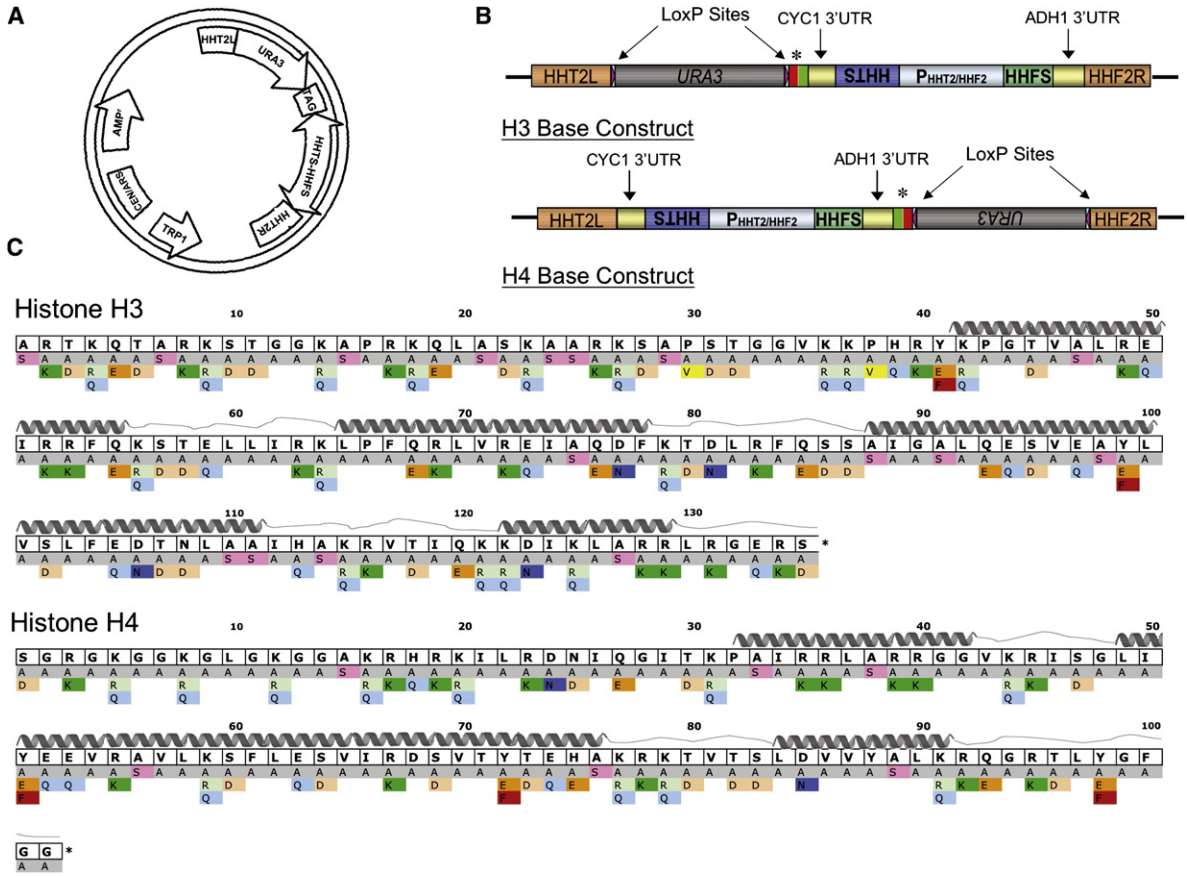

Figure 1. Features of Synthetic Histone Cassette

(A) Schematic representation of histone H3/H4 cassette in pRS414. The two selectable markers, *TRP1* and *URA3,* can be used to select an episomal copy or an integrated cassette, respectively.

(B) Cassettes contain synthetic H3 and H4 genes (*HHTS* and *HHFS*) flanking a central native *HHT2*/*HHF2* promoter region ($P_{HHT2\text{-}HHF2}$). Mutations are engineered into either *HHTS* or *HHFS* and tagged with molecular barcodes (TAGs, labeled *). Upper cassette indicated is used as base construct for *HHTS* (H3) mutants; lower one is used as base construct for *HHFS* (H4) mutagenesis.

(C) The mutant library consists of an alanine scan with other systematic residue swaps and systematic tail deletions, totaling 486 mutants.

fell in alpha helices and tended to be more highly conserved residues (Figure 2C), suggesting that the mutations interfered with nucleosome assembly or histone stability.

Amino acid substitutions that increase net negative surface charge are prominent among the lethal mutants. These fall into two classes; one class is on the DNA-binding (lateral) surface and consists of positively charged residues that when changed to neutral residues is lethal but when changed to other positive residues is not. The second class includes semi-buried uncharged residues near the end of alpha helices in the core; when these residues are changed to acidic residues (but not other neutral residues), lethality can occur. Additionally, 9 of 79 N-terminal tail deletions resulted in lethality in both strains (Figure 2D). The pattern of lethality in histone tails is complex. In histone H3, the two longest tail deletions are inviable, but only in one of two strain backgrounds tested. A single much shorter deletion is inviable in both backgrounds; this protein accumulates at near normal levels, thus lethality presumably results from a toxic junction sequence. In histone H4, the pattern also defies simple explanation, but many of the longer deletions are inviable in both backgrounds; the data suggest that deletion of 4–5 lysine residues is incompatible with viability.

Strain Differences Matter

For the most part, the list of inviable mutations agreed in the two strain backgrounds, with some notable exceptions (Figures 2A and 2D). In a few cases, a lethal mutant in one strain background was "sick" in the other, but in most cases, mutations causing lethality in one background supported near normal growth in the other. These discrepant results between strain backgrounds help explain earlier reports of phenotypic discrepancies in the literature, for example discordant results with histone tail multipoint K to R mutants (Megee et al., 1990; Johnson et al., 1990; Park and Szostak, 1990).

One especially interesting cluster of residues near the C terminus of histone H4 falls into this category, along with some residues essential (or conferring slow growth) in both backgrounds. These include Y88, L90, and Y98. These residues appear to form an important surface *inside* the nucleosome core. Viewing the nucleosome structure from the disk face with the dyad at

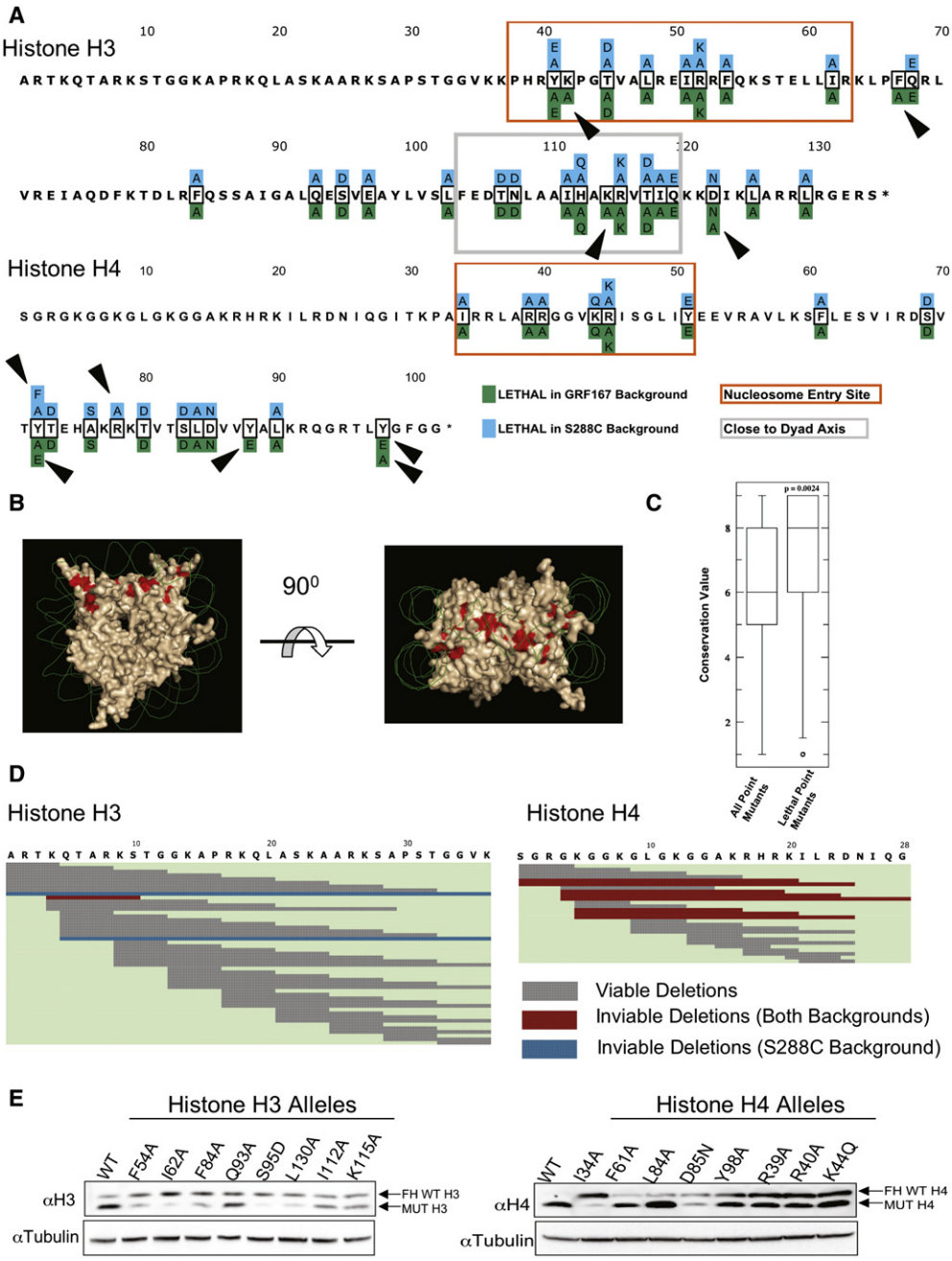

Figure 2. Analysis of Lethal Histone Alleles

(A) Substitution mutations above the sequence are lethal in the S288C strain background (blue); those below are lethal in GRF167 (green). Arrows indicate substitution mutations with strain-specific lethality. Clusters of amino acids at crucial nucleosomal locations are boxed.

(B) Nucleosome view indicating lethal substitutions tracking DNA-binding surface at nucleosome dyad. Only lethal mutants common to both genetic backgrounds are shown.

(C) Correlation between lethal point mutants and evolutionary conservation. Evolutionary conservation scores for each histone residue were calculated using ConSurf. Whiskers in the box and whiskers plot represent minimum and maximum values excluding outliers, defined as 3/2 times higher (or lower) quartile.

(D) Distinct sets of lethal tail deletions in two strain backgrounds. Gray boxes, deleted amino acids in viable mutants; red boxes, deletions lethal in both genetic backgrounds; Blue box, lethal in S288C strain only.

(E) Protein stability of episome-remedial lethal mutants was monitored by immunoblotting. JDY strains expressing indicated lethal mutations were transformed with FLAG-His tagged WT histone (FH-WT) blotted for either anti-histone H3 or anti-histone H4 and anti-tubulin as a loading control. Arrows indicate position of the mutated histone protein (MUT) and tagged WT histone protein. See also Figure S2.

12 o'clock, the upper half of the nucleosome is packed with the H3 H4 tetramer and the H2A C termini and largely solvent free. The lower half of the nucleosome consists of two separate half-disks separated by a water-filled but somewhat tortuous cleft in a castanet-like structure (Figure S1). The residues noted above are part of a surface that forms the base of this cleft; the residues are interwoven with portions of histones H3 and H2B to form this surface. We suggest that these residues could serve as a molecular spring that maintains tensile strength in the lower half of the nucleosome. Tyrosine 88 of H4 stacks on tyrosine 86 of H2B in the structure, forming a spring-like structure (Figure S1B). Whereas mutation to phenylalanine supports viability, a more severe substitution to glutamate does not.

Episome Remediality and Protein Stability of Lethal Mutants

While the number of lethal mutations is small, the number of essential residues detected here is somewhat higher than reported in other studies. The lethal mutants are likely to be lethal for a variety of reasons.

We hypothesized that the slightly higher frequency of lethal mutants observed in this study relates to the fact that the alleles were integrated in single copy as opposed to other studies in which they were maintained episomally; unstable plasmid copy number could potentially mitigate the deleterious effects of a mutated histone, presumably by increased expression as a result of selection for mildly increased copy number. We systematically tested episome remediality of lethal mutations by introducing them on a centromeric plasmid. We found that 25% (14/55) of the point mutants that were lethal in strain JDY23 were episome remedial (Table S1).

We tested protein stability of the lethal mutant histones in the presence of a tagged WT histone (Figures 2E and S2) and found that 35% (12/34) of the H3 and 38% (8/21) of the H4 lethal point mutants led to a significant decrease in protein abundance. Decreased RNA abundance did not explain reduced protein abundance in these mutants (Figure S3). Intriguingly, several of these mutants appear instead to *overproduce* histone mRNA, suggesting regulatory compensation for a histone deficit. All lethal tail deletions showed only minor effects on protein stability. However, many of the lethal mutants produced high levels of protein, and protein was detectable in all of the mutants except H3 D123A/N.

High-Throughput Phenotyping of Individual H3 and H4 Mutants

Phenotypes associated with each of the viable histone mutants in the GRF167 background were determined in thirteen separate assays grouped into five phenotypes: temperature sensitivity, DNA-damage response, transcriptional elongation, transcriptional silencing, and response to microtubule disruption. Cold-sensitive (Cs) alleles were scored at 16°C; temperature-sensitive alleles (Ts) were scored at both 37°C and 39°C. The DNA-damage response was tested in the presence of hydroxyurea (HU), camptothecin (CPT), methyl methanesulfonate (MMS), or UV irradiation. Mutants with potential defects in transcriptional elongation or in their response to microtubule disruption were identified by their sensitivities to 6-azauracil (6AU) or to benomyl, respectively. The role of specific residues in transcriptional silencing was assessed using reporter genes inserted at all three transcriptionally silent regions in yeast, namely the rDNA, the telomeres, and *HMR* loci, as well as by mating competency. Data for the individual mutants in each of these assays are available on the Histone Mutation Database (http://www.histonehits.org) and are visually represented on the nucleosome surface in Figure S3. Most of the histone point mutants had phenotypes in 0–1 classes (defined in Experimental Procedures); few mutants had phenotypes of >3 classes (Figure 3A). Overall agreement with data from previous studies (Hyland et al., 2005; Matsubara et al., 2007) was excellent (Figure S5).

Histone substitutions had the greatest effect on transcriptional silencing with a total of 183 (38%) and 148 (30%) of the alleles displaying altered levels of reporter gene expression from rDNA and telomeric heterochromatic loci, respectively. The assays permitted detection of both increased silencing and loss of silencing, and the results indicate that approximately 80% and 75% of these alleles have a negative influence on rDNA and telomeric silencing, respectively.

Figure 3B illustrates the nucleosomal position of the mutations affecting silencing with a screenshot from http://www.histonehits.org. Histone substitutions on the nucleosome face were significantly enriched for both loss of telomeric silencing (LTS) and loss of *HM* silencing (see *HMR* silencing results, Figure S3I). These residues cluster around the previously identified LRS (loss of rDNA silencing) surface (Park et al., 2002), encircling the H3 K79 methylation site, known to play a role in demarcating euchromatin and heterochromatin (van Leeuwen et al., 2002). At the rDNA, nucleosome surface mutations predominantly lead to an increased rDNA silencing (IRS) phenotype. This is perhaps not surprising given the mechanistic differences underlying rDNA silencing and silencing at the telomeres and *HM* loci. It is striking, however, that this distinction can be manifested in histone mutations at similar nucleosome positions and suggests that heterochromatin structure at these different silent loci varies dramatically. Mutations on the lateral surface show similarly discordant results at telomeric and rDNA loci. These substitutions are statistically enriched for LTS, in addition to IRS phenotypes. Within chromatin, this surface is inaccessible as it lies beneath the DNA helix and presumably anchors histone-DNA interactions. However the different classes of phenotypes arising from alterations in the amino acid composition at this interface would suggest that these residues play more complex roles in formation and maintenance of locus-specific heterochromatin.

The tail deletions showed striking silencing phenotype patterns. Seventy-seven percent of H3 tail deletions have an LRS phenotype whereas only 33% and 8% showed an effect at telomeres and *HMR*, respectively, indicating the main role of the H3 tail in silencing is at the rDNA. The converse pattern of silencing phenotypes was noted in strains expressing deletions in the H4 tail. Nearly 80% of viable H4 tail deletions lost the ability to silence the reporter at both telomeres and at *HMR*, whereas only 17% affected rDNA silencing. These data further extend the discordance between rDNA and telomeric/*HMR* silencing mechanisms and support the hypothesis that they converge on distinct nucleosome domains.

To investigate whether pleiotropy correlates with evolutionary conservation, we used ConSurf (Glaser et al., 2003; Landau

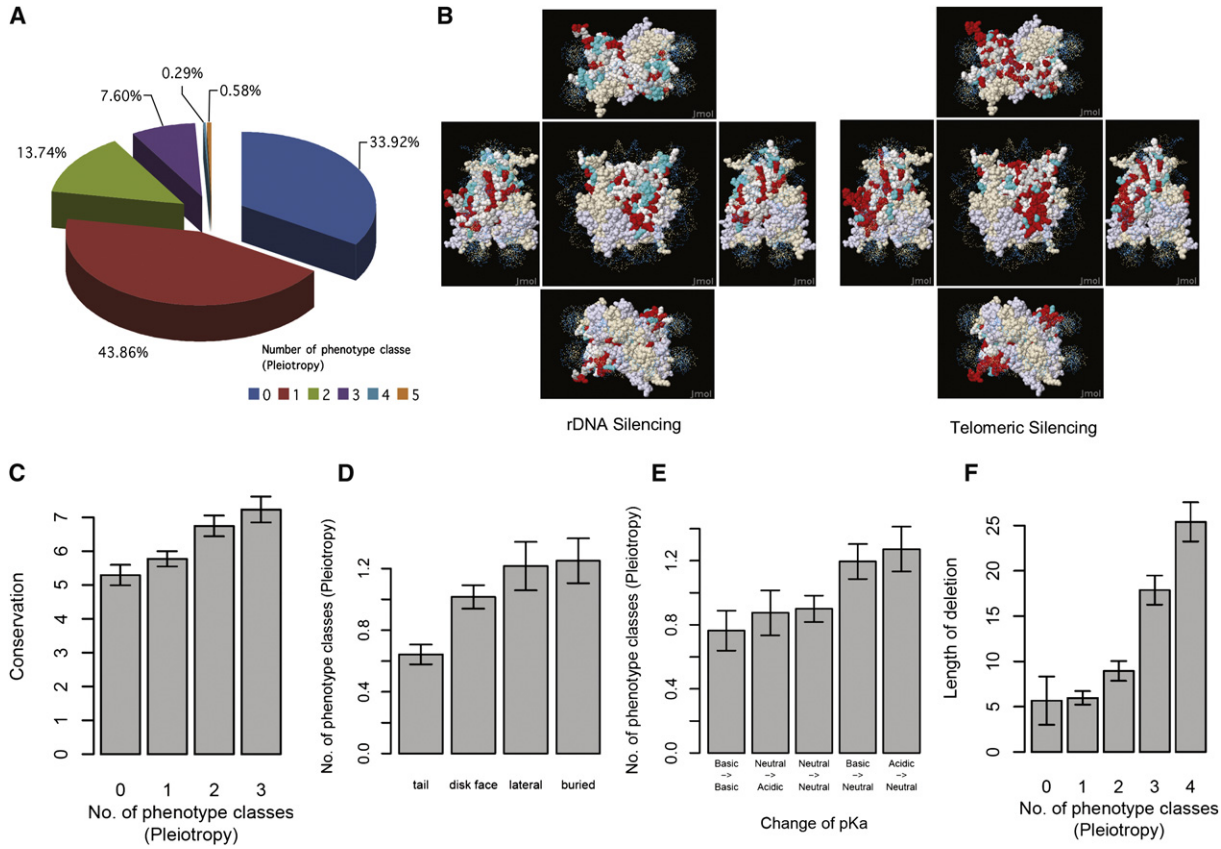

Figure 3. High-Throughput Phenotypic Analysis

(A) Pie chart shows % of mutants with pleiotropy values of 0–5, defined as the number of phenotype classes with at least one non-WT phenotype.

(B) Distinct but overlapping substitution mutations affect transcriptional silencing. Red, mutations losing rDNA or telomeric silencing; aqua, mutations enhancing silencing. Individual residues can be identified by mousing over a region(s) of interest on http://www.histonehits.org.

(C) Evolutionary conservation scores for each residue, calculated using ConSurf, are averaged for mutants binned by pleiotropy.

(D) Average pleiotropy values are shown for mutants binned into four geographical nucleosome domains: tail, disk surface, lateral surface, or buried (Supplemental Experimental Procedures).

(E) Average pleiotropy values are shown for mutants binned by ΔpK_a. Acidic-to-neutral and basic-to-neutral changes are significantly more pleiotropic than basic-to-basic (see text).

(F) Average deletion lengths are shown for tail deletion mutants binned by pleiotropy.

For (C)–(F), vertical bars indicate the standard errors of the binned means.

et al., 2005) to calculate evolutionary conservation scores for each residue, assigning discrete scores from 1 (most variable) to 9 (most conserved). As expected, residues with higher pleiotropy values were significantly more conserved (Figure 3C; $p = 0.005$, one-sided Kendall's rank correlation test).

We explored whether certain phenotypic classes were overrepresented geographically on the nucleosome (Table S2; Supplemental Experimental Procedures). The frequencies of phenotypic values for different domains were significantly different (Figure 3D; $p = 0.001$, Kruskal-Wallis rank sum test). Tail residue mutations are significantly less pleiotropic than mutations in buried regions ($p = 0.004$) or the disk face ($p = 0.004$ and $p = 0.0012$, respectively, two-sided Wilcoxon signed-rank test corrected for multiple comparisons). 6-AU-sensitive mutants were overrepresented on the lateral surface and were absent from the disk face (http://histonehits.org). Temperature-sensitive mutants were overrepresented on the disk face and absent from the tails (Table S2). Figure 3E shows the correlation between phenotypic value frequencies and change in side chain pK_a values (Supplemental Experimental Procedures); different pK_a classes had significantly different numbers of phenotype classes ($p = 0.003$, Kruskal-Wallis rank sum test). Post hoc paired comparisons demonstrated that acid-to-neutral and basic-to-neutral changes were significantly more likely to produce more severe phenotypes than basic-to-basic changes ($p = 0.04$ and 0.03, respectively, two-sided Wilcoxon tests corrected for multiple comparisons). Tail deletions demonstrated a significant correlation between deletion length and pleiotropy (Figure 3F; $p = 2 \times 10^{-12}$, one-sided Kendall's rank correlation test).

Effect of Tail Deletions on Nucleosome Core Modifications

Interdependencies of histone modification sites have been noted previously (Kouzarides, 2007). In parallel work, Nakanishi et al.

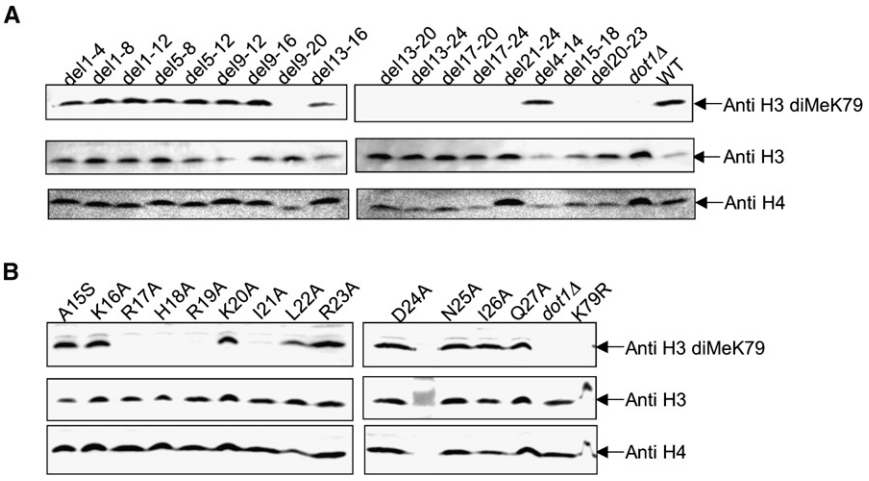

Figure 4. Tail Deletions Affect K79 Methylation

(A) Immunoblots of extracts of cells expressing WT or indicated H4 tail-deletion mutants using antibodies against dimethylated K79 (diMeK79). Antibodies against histone H3 and H4 were used as loading controls; *dot1*Δ strain is the negative control.

(B) Immunoblot analysis as in Figure 4A but with H4 point mutant extracts.

(2008) systematically mapped interdependencies of histone modifications using an alanine scanning substitution series. To test the utility of our resource for discovering interdependencies we probed N-terminal tail requirements for histone H3 acetylation at K56 and methylation at residues K4 and K79.

Immunoblotting was performed on whole-cell extracts from yeast strains harboring viable deletions of histones H3 or H4 (Figure 4A). Every histone H4 tail deletion lacking residues 17 to 23 completely blocked dimethylation of H3 K79. Loss of K79 dimethylation is specific to H4 tail deletions, as none of the H3 tail deletions had this effect (data not shown). The effect of H4 tail deletion on K79 dimethylation is specific; tail deletions affected neither K56 acetylation nor K4 methylation (data not shown). To pinpoint critical residues within H4 important for K79 dimethylation, we exploited the available single point mutations (Figure 4B); mutants R17A, H18A, and R19A completely inhibit K79 dimethylation. Additionally the I21A mutant dramatically, if not completely, blocked modification and L22A had a minor inhibitory effect. These results extend recent reports that basic patch residues (residue 17–20) on histone H4 regulate H3 K79 methylation (Altaf et al., 2007; Fingerman et al., 2007). Our results show clearly that at least one residue (I21) beyond the basic patch residues identified previously is also critical for H3 K79 dimethylation.

Survival of the Fittest—Behavior of the Mutant Pool in a Chemostat

The high level of sequence conservation of histone proteins across phyla suggests a fitness advantage of these particular amino acid sequences during evolution. Yet comprehensive analysis indicates that many histone mutations have no recognized phenotype. To see if some mutants cause subtle fitness reductions, we compared growth over several generations, measuring relative mutant fitness under steady-state growth conditions. We cultured the pool of viable histone mutants in glucose-limiting medium in parallel chemostats, maintaining the population in steady-state exponential growth (Novick and Szilard, 1950). It has previously been shown that glucose-limited chemostat experiments extending >20 generations select for fitter genetic variants, providing a convenient model for adaptive evolution by natural selection (Horiuchi et al., 1962; Paquin and Adams, 1983). After 10 days' growth, (~30 generations), populations were sampled, and amplified TAGs were analyzed. Figure 5A depicts the TAG array intensity ratios on the chemostat samples from days one and ten relative to the original inoculum; red spots indicate reduced hybridization on day 10. Data indicate that ~40% of the viable histone mutants were reduced or eliminated in the pool ($\log_2$ ratio of signal intensity of day 10 versus inoculum < -1.5). Surprisingly, a subset of 27 histone mutants show a higher intensity after growth ($\log_2$ ratio $> +1.5$), suggesting that they are collectively fitter and maintain a selective advantage under glucose limitation. Figure 5B illustrates high concordance between two independently grown chemostats at day 10. We grew the chemostat 10 more days and analyzed this population. Figures 5C and 5D show allele distributions in chemostats on days 10 and 20, respectively. Mutants were grouped and colored based on their day 10 abundance. Figure 5D shows that most mutants are reduced in the population after 20 days; most of those that thrive after 20 days were already abundant at day 10 (Table S3); thus these strains exhibit a fitness advantage over the other mutants. Indeed 8 out of the 27 day 10 "winners" still dominate the population at day 20.

To determine whether the winner histone mutations accounted for their success in the chemostat we cultured the unevolved day 10 winning histone mutants in the presence of WT for 30 generations. Each histone mutant was represented at the same level as WT in the initial inoculum. Figure 5E indicates that the winner histone mutants had outcompeted WT by day 10, equating to ~6% faster growth under these conditions.

Analysis of Double Mutants

SLAM is a high-throughput technology for identifying genetic interactions. SLAM was used to probe synthetic gene interactions between the histone mutant library and two genes encoding key regulators of chromatin biology, *UBP8* and *SET2*. These regulators control the levels of H2B K123 ubiquitylation (K123Ub) and H3 K36 methylation, respectively. We hypothesized that the ability of a cell to respond to perturbed modification, through the deletion of these loci, may depend on processes involving other key histone residues. To probe this, the histone mutant library was transformed with specific *kanMX* targeting constructs, and histone tags were amplified and analyzed. The intensities of each histone mutant TAG on the array were compared with those amplified from a control histone library with a deletion at a

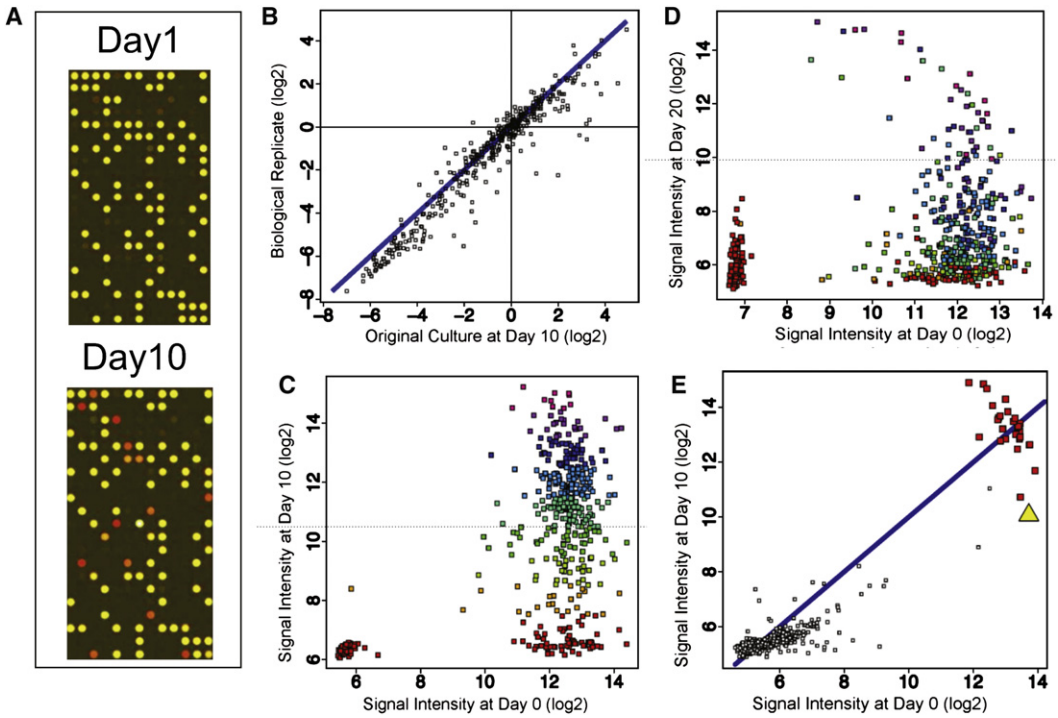

Figure 5. Chemostat Growth Profiles Reveal Subset of Mutants that Outgrow Wild-Type

Cells were cultured in a glucose-limited chemostat at 30°C and sampled as indicated.

(A) Microarray ratio images. Red features represent mutants depleted after chemostat.

(B) Reproducibility of chemostat growth profiles. Two independent chemostat cultures were grown in parallel to day 10. The $\log_2$ ratios express relative enrichment of mutants.

(C) Chemostat population profile at day 10. Scatter plot depicts $\log_2$ signal intensity associated with each mutant before (*x* axis) and after (*y* axis) growth; colors stratify mutant population by relative abundance.

(D) Population profile at day 20; color assignments as in (C).

(E) Chemostat growth of overrepresented mutants. Mutants from the top strata of C were cocultured as above for 10 days in competition with a matched WT strain. Changes in $\log_2$ signal intensity are depicted as in (C). Yellow triangle, WT. Small open squares, mutants not present in this experiment.

"neutral" locus, *HO*. Figure 6A plots log ratios of the TAGs in *ubp8Δ::kanMX* relative to *hoΔ::kanMX* for viable mutants. Two synthetic fitness (SF) interactions with *ubp8Δ* were validated, H3 K56Q and H4 K91A (Figure 6B). These double mutant combinations resulted in an SF interaction; the double mutant grew but exceedingly poorly. Direct testing revealed three additional interactions with the H3 K56R, H3 K56A, and H4 K91R alleles (not shown). It is striking to note that both H3 K56 and H4 K91 are potentially acetylated residues situated within the nucleosome globular core (Masumoto et al., 2005; Xu et al., 2005; Ye et al., 2005), suggesting a functional interaction between these histone marks and Ubp8p. Since deubiquitylation of histone H2B K123 by Ubp8p is a key regulatory step in the switch from transcription initiation to elongation (Wyce et al., 2007; Henry et al., 2003), K56 and/or K91 modification status may affect the transcription cycle.

We also identified three histone alleles, H3 T107A, H3 K9A, and H3 Del [9–20], that reproducibly gave rise to SF defects in a *set2*Δ background (Figure 6C). H3 T107 is buried within the core of the nucleosome close to the dyad axis and has no known biological role to date. Both the H3 K9A and H3 Del [9–20] alleles eliminate H3 K9 acetylation, a mark required for transcriptional activation. Eliminating both these marks is detrimental and may suggest a role for H3 K9 acetylation in normal chromatin function in the absence of Set2p methylation.

H3 Tail and NHEJ

The DNA double-strand break (DSB) is a toxic DNA lesion resulting from environmental stress, chemical insult, or stalled replication forks. To probe histone requirements for DSB repair, we applied our histone mutant pool to study the nonhomologous end joining (NHEJ) pathway using a transformation-based plasmid repair assay (Ooi et al., 2001). A number of mutants showed apparent NHEJ defects, including several N-terminal tail mutants of histone H3 (Figure 6D and Table S4). Six mutants significantly defective in NHEJ were individually confirmed; NHEJ efficiency in these was ~1/3 that of WT and about 4-fold higher than that of a *lig4* control strain (Figure 6E). One striking finding is that most of the H3 tail deletions appear defective in NHEJ repair. In contrast, only a small number of tail deletions on histone H4 have this effect, suggesting a specific role for the H3 tail in NHEJ. Other mutations affecting NHEJ include H3 K56, an important site of acetylation. Although K56R only modestly affects NHEJ (Masumoto et al., 2005), a recent report demonstrated that

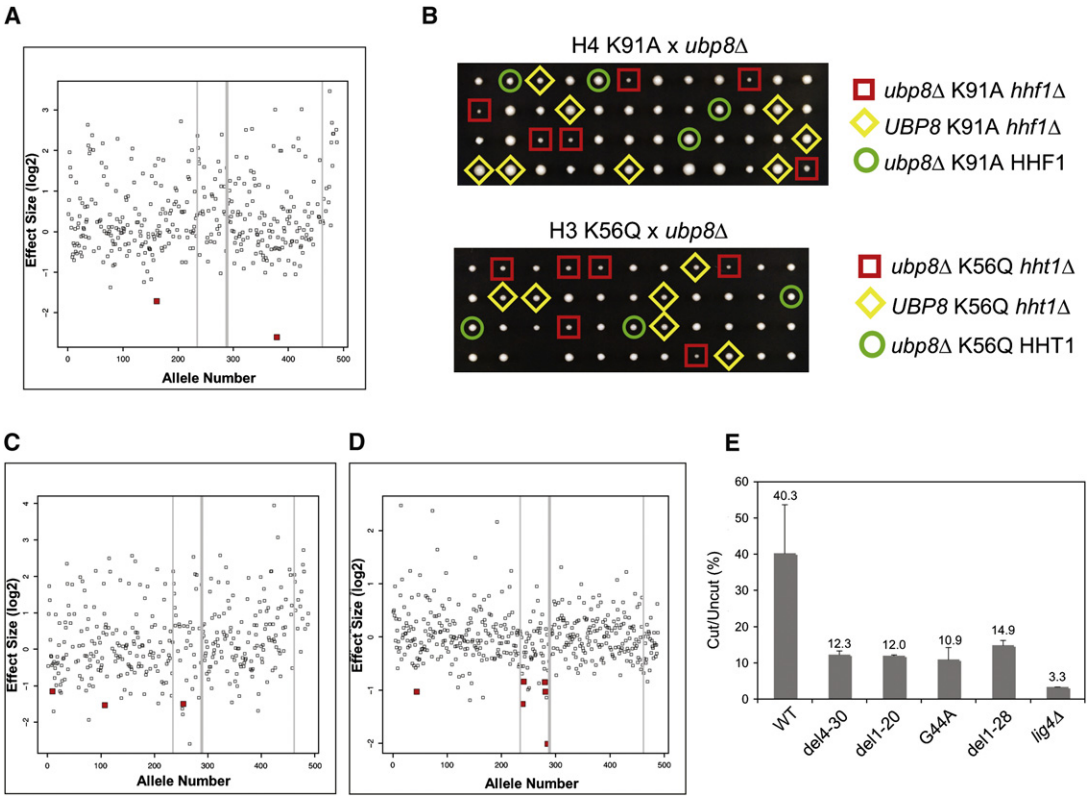

Figure 6. Assaying Complex Phenotypes using TAG Arrays

(A) Double mutant analysis of histone library with *ubp8*Δ. Scatter plot depicting $\log_2$ ratio of abundance of each mutant in a *ubp8*Δ strain. Gray vertical lines (alleles 235–288 and 461–488) separate allelic classes (left to right: H3 substitutions, H3 deletions, H4 substitutions, H4 deletions). Red squares identify substitution mutants verified individually for synthetic interactions.

(B) Tetrad analysis to determine viability. Haploid strains carrying *ubp8⊿* or the indicated histone mutation were mated for 4 hr, and then diploids were purified and sporulated. Tetrads were dissected on YPD medium to score fitness defects. Relevant genotypes are indicated.

(C) Double mutant analysis of histone library with *set2*Δ. Scatter plot as in (A), depicting $\log_2$ ratios in a *set2*Δ strain.

(D) Analysis of NHEJ phenotypes. Scatter plot indicating the $\log_2$ ratio of signal intensities of cut/uncut plasmid transformations for each mutant; annotations as in (A).

(E) Individual quantification of transformant recovery of indicated H3 mutant strains transformed with digested plasmid relative to a nondigested control; *lig4⊿* strain serves as a negative control. Error bars represent standard error of the mean.

loss of Rtt109p, the K56 acetyltransferase, impairs NHEJ (Jessulat et al., 2008), consistent with our results. Other histone mutants significantly affecting NHEJ are listed in Table S4. It has been reported that lysine 16 on histone H4 is deacetylated in a *SIN3*-dependent manner in the vicinity of DNA DSBs. Deletion of *SIN3* or *RPD3* confers an NHEJ defect, presumably due to the inability to remove H4 K16 acetylation (Jazayeri et al., 2004). Consistent with this, K16Q, which mimics acetylation (but not K16R), is also defective in NHEJ.

DISCUSSION

Transcriptional Silencing Defects of Histone Mutants

Histones are the key architectural proteins that package the genome, so it is natural to expect that altering histones sequences will impact the structure of chromatin. Transcriptionally silenced heterochromatic loci provide a genetically tractable system for monitoring chromatin structure. Indeed the histone substitutions collectively had a greater effect on transcriptional silencing than any other phenotype class scored. Point mutations leading to silencing defects at telomeres and the *HM* (homothallic mating) loci were enriched on the LRS (Park et al., 2002) nucleosome surface near methylated residue H3 K79. K79 methylation regulates the recruitment of Sir3p, a protein that is central to the establishment of silencing at telomeres and the *HM* loci and that directly interacts with this nucleosomal surface (Onishi et al., 2007; A. Norris and J.D.B., unpublished data). Therefore these histone alleles may perturb telomeric and *HM* silencing by destabilizing Sir3p binding through effects on H3 K79 methylation. Interestingly, however, mutations at many of these same residues cause *increased* rDNA silencing. *HM* and telomeric silencing requires the Sir2p, Sir3p, and Sir4p complex whereas rDNA silencing depends solely on Sir2p (Bryk et al., 1997; Smith and Boeke, 1997). Perhaps Sir3p destabilization at telomeres/*HM* by a given histone mutation increases the pool of Sir2p available to bind to rDNA, enhancing rDNA silencing (Smith et al., 1998).

The distinct effects of histone H3 and H4 N-terminal deletions at silent loci (as in NHEJ) indicate that the flexible tails play

distinct roles at telomeres/*HM* and rDNA. rDNA silencing requires histone H3 residues 4–20 whereas alleles that remove residues 21–36 have no phenotype and behave similarly to WT. Recent work (Bryk et al., 2002; Fingerman et al., 2005) implicated histone H3 K4 methylation by Set1p in rDNA silencing. However, loss of this methylation site cannot account for our entire dataset because certain deletion alleles with an LRS phenotype do not span K4. Thus the mechanisms underlying these rDNA silencing defects are complex.

Interactions among Nucleosome Regions

The combination of histone point and deletion mutants provides a powerful screening tool for identifying interdependencies among different nucleosome regions with regard to modifications. Here we probed three different lysine modifications by screening for the effects of histone tail deletions. The first two were unaffected by deletion histone tails. However, K79 dimethylation was much decreased in a subset of H4 tail deletions. Recent studies implicated a basic patch (residues 17–20) in the H4 tail in Sir3p binding and Dot1p histone H3 K79 di- and trimethylation (Altaf et al., 2007; Fingerman et al., 2007; Onishi et al., 2007). Specifically, it was proposed that both Sir3p and Dot1p compete for the same target at the nucleosome surface, thereby determining local hetero/euchromatin status. Using our library, we identified two regions in the H4 N-tail required for modification. An in vitro study showed that Sir3 bound to a longer histone H4 peptide (residue 1–34) but not a shorter one (residue 1–20) (Onishi et al., 2007), suggesting that additional residues in the histone H4 tail may facilitate Sir3p binding. The I21-L22 residues could mediate this interaction. Alternatively, these residues may affect Dot1p binding. Consistent with these hypotheses, mutations in both residues have significant telomeric silencing defects, similar to those observed in *sir3* or *dot1* deletion strains. Further investigation is needed to differentiate whether the effect is on Dot1p, Sir3p, or both; the mutant resource will be useful in dissecting these interactions.

Assaying Complex Phenotypes using TAG Arrays

The chemostat and NHEJ studies show that the mutant resource can be used to profile subtle quantitative phenotypes. In the chemostat, in addition to defining less fit mutants, a small but surprising cohort of mutants was identified that were fitter than the WT histone. Two hypotheses we considered to explain this observation are (1) these adapted strains are intrinsically fitter than WT under glucose limitation, or (2) they had acquired beneficial mutation(s) during the experiment, a typical characteristic of strains grown continuously under suboptimal conditions (Paquin and Adams, 1983). We explored the possibility that mutation rate in these histone mutant strains was elevated but found that the winning histone mutant strains were not significantly different from WT (Figure S4). It is interesting to note that ~35% of the winning substitutions are at modified residues known to be important for transcription. We therefore favor the explanation that these histone substitutions are inherently more capable of adapting to the growth condition used, perhaps through altered transcriptional remodeling. In support of this, significant gene expression changes in *S. cerevisiae* are seen in glucose limited chemostats (Ferea et al., 1999).

Our efforts to probe for functions of H3 and H4 residues in specific genetic backgrounds using SLAM uncovered new connections between known histone modifications. One of the more surprising insights is the sensitivity of *upb8* mutants to H3 K56 mutations. Consistent with this, Collins et al. (2007) report phenotypic enhancement of *ubp8*Δ by *hst3*Δ, one of the redundant deacetylases controlling K56 acetylation (Celic et al., 2006; Maas et al., 2006). This indicates that phenotypes associated with *UBP8* deletion can be suppressed by increasing K56Ac levels, suggesting that our SF interaction results from loss of K56Ac. An SF defect was found between *ubp8*Δ and both H4 K91A and H4 K91R, but not H4 K91Q. This latter allele mimics a constitutively acetylated form of H4 K91 and therefore our result is consistent with a model in which cells lacking *UBP8* require H4 K91Ac. Since mutations at both H3 K56 and H3 K91 are known to perturb genome stability, we speculate that *UBP8* may be involved in cellular recovery from genomic stress.

DSBs are dangerous DNA lesions and repaired by two major pathways: homologous recombination (HR) and NHEJ. In the past few years, many covalent modifications on histones were implicated in DSB repair, including phosphorylation (Downs et al., 2007), acetylation (Jazayeri et al., 2004), methylation (Huyen et al., 2004) and ubiquitylation (Kamiya et al., 2007). Using the mutant library, we found many new histone mutants defective in NHEJ.

Most H3 tail deletions are NHEJ defective. Consistent with this, H3 tail lysine mutations affect or partially affect both HR and NHEJ (Qin and Parthun, 2002). We observe specific NHEJ requirement for the H3 tail, suggesting a stimulatory interaction with required NHEJ components or exclusion of an NHEJ inhibitor. The silent chromatin components, Sir2p, Sir3p, and Sir4p, are also required for efficient NHEJ (Tsukamoto et al., 1997). However, their effect on NHEJ is primarily indirect, resulting from desilencing of silent mating-type genes (Lee et al., 1999). The H3 tail could affect the NHEJ pathway indirectly, in a way similar to Sir proteins. This may be true in part but not for all H3 tail deletions observed since only a few of these deletions display significant mating defects (http://www.histonehits.org). Moreover H4 tail deletions compromise mating but not NHEJ. H3 tail deletions could affect expression of NHEJ components. Microarray data indicate that the H3 tail represses gene expression dramatically (Sabet et al., 2003; Yu et al., 2006). However no significant downregulation of NHEJ components was described in these papers, suggesting a different mechanism. We favor the hypothesis that the H3 tail mediates specific interactions with a key NHEJ pathway component.

A Paradigm for High-Throughput Structure/Function Analysis of Protein Complexes

The paradigm by which we systematically mutagenized the H3 and H4 proteins can be adapted to any protein or protein complex in yeast. Judicious use of synthetic DNA fragments facilitates construction of very flexible analysis cassettes that can be used in multiple genetic contexts. The tagging strategy allows existing microarray formats with known and tested hybridization properties to be reused in new ways. More importantly, it allows the massively multiplexed collection of data on complex phenotypes such as evolutionary competitiveness or interactions with

hundreds or thousands of other mutants. We envision extending the approach outlined here to comprehensive screening of genes using eMAP approaches (Collins et al., 2007; Schuldiner et al., 2005) as well as SLAM. The combination of systematic and well-organized genetic/functional/phenotypic data with 3D structural information in the context of sophisticated database queries is a powerful tool to assimilate comprehensive data on a complex-by-complex basis.

EXPERIMENTAL PROCEDURES

Construction of Bacterial and Yeast Libraries of 486 Mutants

Mutant constructs were synthesized and cloned into pRS414 by GeneArt Inc. (Regensburg, Germany; http://www.geneart.com) and supplied as bacterial stocks. Plasmids were isolated and digested by BciVI digestion, releasing the construct from the plasmid backbone, and were transformed into yeast with uracil selection as described (Pan et al., 2007). Two independent colonies were isolated for each construct and streaked onto SC−Ura to obtain single colonies (see Supplemental Experimental Procedures for details of strains, plasmids, and media). Cells were transferred to α-amino-adipate medium (Chattoo et al., 1979) to segregate the pJP11 [*LYS2 HHT1 HHF1*] episomal plasmid to preliminarily identify lethal mutants. Mutants unable to give rise to resistant clones on α-amino-adipate were tested further by replica plating on SC−Lys and SC−Trp following nonselective growth. Correct integration was confirmed by colony PCR. Confirmed viable mutants (able to grow in the absence of pJP11) were frozen in 96-well plates in the same format as the original collection. Lethal mutants (unable to segregate pJP11) were frozen separately in 96-well plates. The viable mutants in JDY86 were pooled as previously described (Pan et al., 2007).

Library Validation

Libraries were validated in three steps: (1) each mutant was constructed, transformed into bacteria, and sequenced; 100% sequence identity was required to pass quality control; (2) after plasmid isolation from yeast, 5–10 randomly selected constructs from each 96-well plate were sequenced to ensure the identity of each mutant in the well and no crosscontamination during plasmid preparation; 100% of these were correct; (3) after we obtained the yeast library, we PCR-amplified the individual integrated constructs followed by sequencing to confirm the identity of mutations. This last step was performed for all the lethal mutants.

Chemostat Competition Experiments

The viable histone mutant library in the JDY86 background was cultured in two aerobic glucose-limited (0.08%) YNB medium (supplemented with 40 mM tryptophan, 50 mM methionine, 100 mM leucine, and 100 mM lysine) chemostats at 30°C for 10 or 20 days. The initial inoculum contained ~10^9 cells, with each mutant roughly equally represented; dilution rates were maintained at 0.2 h^{-1}. For competition experiments, two colonies from each strain were spotted on SC plates and grown overnight at 30°C scraped from the plate and pooled.

NHEJ Assays

Pools of mutants were made competent and transformed with uncut and HindIII-digested pRS415 in parallel. ~10^6 to 10^7 cells were spread on two 150 mm plates containing SC−Ura−Leu. After incubation at 30C for 2 days, these plates were replicated onto new SC−Ura−Leu plates for another day before the cells were scraped and pooled and genomic DNA was extracted. To confirm the microarray data, individual 5 ml cultures were grown at 30°C in YPD, then inoculated into fresh medium and grown to A_{600} = 0.6. Cells were transformed with uncut or HindIII-digested pRS415 and plated on SC−Leu. Plates were incubated at 30°C for 2 days before counting. Repair efficiency of NHEJ is expressed as linear/uncut ratio of Leu^+ transformants. Values represent the average of two independent experiments performed in quadruplicate.

Design of the Array

Histone TAG Arrays are a repurposing of a microarray design originally created to represent the TAG sequences in the Yeast Knockout collection (Yuan et al., 2005; NCBI GEO Accession Number GPL1444). The TAG sequences used were those assigned to five-way replicate features in the design. Each of the 48 histone H3 or H4 mutants was consecutively assigned a pair of TAG sequences distinguished as "UpTag" and "DnTag," with the mutants ordered by ID and the sequences ordered by the open reading frame (ORF) represented in the original design. (The H3 Del [1–20] and H3 Del [1–28] mutations are each represented by two mutants.) Sequences were skipped if they introduced any of the restriction sites reserved for cloning purposes (BciVI, SacI, SacII, SalI, XhoI, NotI, KpnI, BglII, ClaI, NheI). The WT construct was assigned UpTag and DnTag sequences given by IDs 11046 and 10995, respectively. Due to an oversight, the UpTag was later also assigned as the DnTag for the histone H3 G13A mutation.

PCR Amplification of TAG Sequences

The yeast knockout universal primer sequences were modified and renamed to avoid restriction sites reserved for cloning and to reduce propensity of primer-dimer formation as follows:

U1h = -ATGTCCACGAGGTCTCT
U1 = GATGTCCACGAGGTCTCT (original)
U2h = CCTCGACCTGCAGCGTA
U2c = -gTCGACCTGCAGCGTACG (original)
D1h = CGGTGTCGGTCTCGTAG
D1 = CGGTGTCGGTCTCGTAG (original)
D2h = CCCAGCTCGAATTCATC
D2c = -CgAGCTCGAATTCATCGAT (original)

Analysis of Histone TAG Array Data

Microarray images and datafiles were acquired using a GenePix 4000B scanner and GenePix Pro 6.1 software (MDS Analytical Technologies, Sunnyvale, CA, formerly Axon Instruments). Datafiles were subjected to spatial normalization using the *hoptag* R package (Yuan and Irizarry, 2006). Using ad hoc R functions (available on request), feature data for each histone mutant were extracted, reduced to their medians, and corrected for a baseline signal intensity derived from the nonhistone features in the array. Because the assumptions underlying loess normalization could not be justified, systematic intensity differences between the Red (Cy5) and Green (Cy3) microarray channels were corrected by subtracting estimates based on the estimated mode of the strongest signals. These corrections were checked using scatter plots of the intensity data for the two channels. Data in which neither channel exceeded 2.0 $\log_2$ units over baseline were regarded as missing. UpTag and DnTag data were averaged if both values were available and within 2.0 $\log_2$ units of each other; otherwise, the larger value was used. Variability was estimated by comparing the UpTag and DnTag values. Data quality was further analyzed as described in Supplemental Experimental Procedures.

ACCESSION NUMBERS

The histone TAG array platform and the datasets described in this paper are available from http://www.ncbi.nlm.nih.gov/geo/ under accession numbers GPL6574 and GSE10860, respectively.

SUPPLEMENTAL DATA

Supplemental Data include Supplemental Text, Supplemental Experimental Procedures, eight figures, and five tables and can be found with this article online at http://www.cell.com/cgi/content/full/134/6/1066/DC1/.

ACKNOWLEDGMENTS

J.D. and E.M.H. contributed equally and are listed alphabetically. We thank Jeffry Corden and Lisa Scheifele for help with chemostats, Anne Norris for discussions and assistance with molecular graphics, and Lisa Chengran Huang, Qing Huang, and Yu-yi Lin for assistance with phenotypic screening. We thank Alain Verreault and Yi Zhang for providing antibodies. This work was supported in part by NIH Roadmap grant U54 RR020839 to J.S.B. and J.D.B.

Received: March 10, 2008
Revised: June 3, 2008
Accepted: July 14, 2008
Published: September 18, 2008

REFERENCES

Adkins, M.W., Carson, J.J., English, C.M., Ramey, C.J., and Tyler, J.K. (2007). The histone chaperone anti-silencing function 1 stimulates the acetylation of newly synthesized histone H3 in S-phase. J. Biol. Chem. *282*, 1334–1340.

Altaf, M., Utley, R.T., Lacoste, N., Tan, S., Briggs, S.D., and Cote, J. (2007). Interplay of chromatin modifiers on a short basic patch of histone H4 tail defines the boundary of telomeric heterochromatin. Mol. Cell *28*, 1002–1014.

Berger, S.L. (2007). The complex language of chromatin regulation during transcription. Nature *447*, 407–412.

Bryk, M., Banerjee, M., Murphy, M., Knudsen, K.E., Garfinkel, D.J., and Curcio, M.J. (1997). Transcriptional silencing of Ty1 elements in the RDN1 locus of yeast. Genes Dev. *11*, 255–269.

Bryk, M., Briggs, S.D., Strahl, B.D., Curcio, M.J., Allis, C.D., and Winston, F. (2002). Evidence that Set1, a factor required for methylation of histone H3, regulates rDNA silencing in *S. cerevisiae* by a Sir2-independent mechanism. Curr. Biol. *12*, 165–170.

Celic, I., Masumoto, H., Griffith, W.P., Meluh, P., Cotter, R.J., Boeke, J.D., and Verreault, A. (2006). The sirtuins hst3 and Hst4p preserve genome integrity by controlling histone h3 lysine 56 deacetylation. Curr. Biol. *16*, 1280–1289.

Chattoo, B.B., Sherman, F., Azubalis, D.A., Fjellstedt, T.A., Mehnert, D., and Ogur, M. (1979). Selection of lys2 mutants of the yeast *S. cerevisiae* by the utilization of alpha-aminoadipate. Genetics *93*, 51–65.

Cheung, W.L., Turner, F.B., Krishnamoorthy, T., Wolner, B., Ahn, S.H., Foley, M., Dorsey, J.A., Peterson, C.L., Berger, S.L., and Allis, C.D. (2005). Phosphorylation of histone H4 serine 1 during DNA damage requires casein kinase II in *S. cerevisiae*. Curr. Biol. *15*, 656–660.

Collins, S.R., Miller, K.M., Maas, N.L., Roguev, A., Fillingham, J., Chu, C.S., Schuldiner, M., Gebbia, M., Recht, J., Shales, M., et al. (2007). Functional dissection of protein complexes involved in yeast chromosome biology using a genetic interaction map. Nature *446*, 806–810.

Downs, J.A., Nussenzweig, M.C., and Nussenzweig, A. (2007). Chromatin dynamics and the preservation of genetic information. Nature *447*, 951–958.

Ferea, T.L., Botstein, D., Brown, P.O., and Rosenzweig, R.F. (1999). Systematic changes in gene expression patterns following adaptive evolution in yeast. Proc. Natl. Acad. Sci. USA *96*, 9721–9726.

Fingerman, I.M., Wu, C.L., Wilson, B.D., and Briggs, S.D. (2005). Global loss of Set1-mediated H3 Lys4 trimethylation is associated with silencing defects in *S. cerevisiae*. J. Biol. Chem. *280*, 28761–28765.

Fingerman, I.M., Li, H.C., and Briggs, S.D. (2007). A charge-based interaction between histone H4 and Dot1 is required for H3K79 methylation and telomere silencing: identification of a new trans-histone pathway. Genes Dev. *21*, 2018–2029.

Glaser, F., Pupko, T., Paz, I., Bell, R.E., Bechor-Shental, D., Martz, E., and Ben-Tal, N. (2003). ConSurf: identification of functional regions in proteins by surface-mapping of phylogenetic information. Bioinformatics *19*, 163–164.

Güldener, U., Heinisch, J., Koehler, G.J., Voss, D., and Hegemann, J.H. (2002). A second set of loxP marker cassettes for Cre-mediated multiple gene knockouts in budding yeast. Nucleic Acids Res. *30*, e23.

Henry, K.W., Wyce, A., Lo, W.S., Duggan, L.J., Emre, N.C., Kao, C.F., Pillus, L., Shilatifard, A., Osley, M.A., and Berger, S.L. (2003). Transcriptional activation via sequential histone H2B ubiquitylation and deubiquitylation, mediated by SAGA-associated Ubp8. Genes Dev. *17*, 2648–2663.

Horiuchi, T., Tomizawa, J.I., and Novick, A. (1962). Isolation and properties of bacteria capable of high rates of beta-galactosidase synthesis. Biochim. Biophys. Acta *55*, 152–163.

Huyen, Y., Zgheib, O., Ditullio, R.A., Jr., Gorgoulis, V.G., Zacharatos, P., Petty, T.J., Sheston, E.A., Mellert, H.S., Stavridi, E.S., and Halazonetis, T.D. (2004). Methylated lysine 79 of histone H3 targets 53BP1 to DNA double-strand breaks. Nature *432*, 406–411.

Hyland, E.M., Cosgrove, M.S., Molina, H., Wang, D., Pandey, A., Cotter, R.J., and Boeke, J.D. (2005). Insights into the role of histone H3 and histone H4 core modifiable residues in *S. cerevisiae*. Mol. Cell. Biol. *25*, 10060–10070.

Jazayeri, A., McAinsh, A.D., and Jackson, S.P. (2004). *S. cerevisiae* Sin3p facilitates DNA double-strand break repair. Proc. Natl. Acad. Sci. USA *101*, 1644–1649.

Jenuwein, T., and Allis, C.D. (2001). Translating the histone code. Science *293*, 1074–1080.

Jessulat, M., Alamgir, M., Salsali, H., Greenblatt, J., Xu, J., and Golshani, A. (2008). Interacting proteins Rtt109 and Vps75 affect the efficiency of non-homologous end-joining in *S. cerevisiae*. Arch. Biochem. Biophys. *469*, 157–164.

Johnson, L.M., Kayne, P.S., Kahn, E.S., and Grunstein, M. (1990). Genetic evidence for an interaction between SIR3 and histone H4 in the repression of the silent mating loci in *S. cerevisiae*. Proc. Natl. Acad. Sci. USA *8*, 6286–6290.

Kamiya, K., Sakakibara, K., Ryer, E.J., Hom, R.P., Leof, E.B., Kent, K.C., and Liu, B. (2007). Phosphorylation of the cyclic AMP response element binding protein mediates transforming growth factor beta-induced downregulation of cyclin A in vascular smooth muscle cells. Mol. Cell. Biol. *27*, 3489–3498.

Klose, R.J., and Zhang, Y. (2007). Regulation of histone methylation by demethylimination and demethylation. Nat. Rev. Mol. Cell Biol. *8*, 307–318.

Kouzarides, T. (2007). Chromatin modifications and their function. Cell *128*, 693–705.

Landau, M., Mayrose, I., Rosenberg, Y., Glaser, F., Martz, E., Pupko, T., and Ben-Tal, N. (2005). ConSurf 2005: the projection of evolutionary conservation scores of residues on protein structures. Nucleic Acids Res. *33*, W299–W302.

Lee, S.E., Paques, F., Sylvan, J., and Haber, J.E. (1999). Role of yeast SIR genes and mating type in directing DNA double-strand breaks to homologous and non-homologous repair paths. Curr. Biol. *9*, 767–770.

Maas, N.L., Miller, K.M., DeFazio, L.G., and Toczyski, D.P. (2006). Cell cycle and checkpoint regulation of histone H3 K56 acetylation by Hst3 and Hst4. Mol. Cell *23*, 109–119.

Masumoto, H., Hawke, D., Kobayashi, R., and Verreault, A. (2005). A role for cell-cycle-regulated histone H3 lysine 56 acetylation in the DNA damage response. Nature *436*, 294–298.

Matsubara, K., Sano, N., Umehara, T., and Horikoshi, M. (2007). Global analysis of functional surfaces of core histones with comprehensive point mutants. Genes Cells *12*, 13–33.

Megee, P.C., Morgan, B.A., Mittman, B.A., and Smith, M.M. (1990). Genetic analysis of histone H4: essential role of lysines subject to reversible acetylation. Science *247*, 841–845.

Morillon, A., Karabetsou, N., Nair, A., and Mellor, J. (2005). Dynamic lysine methylation on histone H3 defines the regulatory phase of gene transcription. Mol. Cell *18*, 723–734.

Nakanishi, S., Sanderson, B.W., Delventhal, K.M., Bradford, W.D., Staehling-Hampton, K., and Shilatifard, A. (2008). A comprehensive library of histone mutants identifies nucleosomal residues required for H3K4 methylation. Nat. Struct. Mol. Biol. *15*, 881–888.

Natsume, R., Eitoku, M., Akai, Y., Sano, N., Horikoshi, M., and Senda, T. (2007). Structure and function of the histone chaperone CIA/ASF1 complexed with histones H3 and H4. Nature *446*, 338–341.

Nelson, C.J., Santos-Rosa, H., and Kouzarides, T. (2006). Proline isomerization of histone H3 regulates lysine methylation and gene expression. Cell *126*, 905–916.

Ng, H.H., Feng, Q., Wang, H., Erdjument-Bromage, H., Tempst, P., Zhang, Y., and Struhl, K. (2002). Lysine methylation within the globular domain of histone H3 by Dot1 is important for telomeric silencing and Sir protein association. Genes Dev. *16*, 1518–1527.

Novick, A., and Szilard, L. (1950). Description of the chemostat. Science *112*, 715–716.

Onishi, M., Liou, G.G., Buchberger, J.R., Walz, T., and Moazed, D. (2007). Role of the conserved Sir3-BAH domain in nucleosome binding and silent chromatin assembly. Mol. Cell *28*, 1015–1028.

Ooi, S.L., Shoemaker, D.D., and Boeke, J.D. (2001). A DNA microarray-based genetic screen for nonhomologous end-joining mutants in *S. cerevisiae*. Science *294*, 2552–2556.

Ooi, S.L., Shoemaker, D.D., and Boeke, J.D. (2003). DNA helicase gene interaction network defined using synthetic lethality analyzed by microarray. Nat. Genet. *35*, 277–286.

Ozdemir, A., Masumoto, H., Fitzjohn, P., Verreault, A., and Logie, C. (2006). Histone H3 lysine 56 acetylation: a new twist in the chromosome cycle. Cell Cycle *5*, 2602–2608.

Pan, X., Yuan, D.S., Ooi, S.L., Wang, X., Sookhai-Mahadeo, S., Meluh, P., and Boeke, J.D. (2007). dSLAM analysis of genome-wide genetic interactions in *S. cerevisiae*. Methods *41*, 206–221.

Paquin, C.E., and Adams, J. (1983). Relative fitness can decrease in evolving asexual populations of S. cerevisiae. Nature *306*, 368–370.

Park, J.H., Cosgrove, M.S., Youngman, E., Wolberger, C., and Boeke, J.D. (2002). A core nucleosome surface crucial for transcriptional silencing. Nat. Genet. *32*, 273–279.

Park, E.C., and Szostak, J.W. (1990). Point mutations in the yeast histone H4 gene prevent silencing of the silent mating type locus *HML*. Mol. Cell. Biol. *10*, 4932–4934.

Qin, S., and Parthun, M.R. (2002). Histone H3 and the histone acetyltransferase Hat1p contribute to DNA double-strand break repair. Mol. Cell. Biol. *22*, 8353–8365.

Sabet, N., Tong, F., Madigan, J.P., Volo, S., Smith, M.M., and Morse, R.H. (2003). Global and specific transcriptional repression by the histone H3 amino terminus in yeast. Proc. Natl. Acad. Sci. USA *100*, 4084–4089.

Sauer, B. (1987). Functional expression of the cre-lox site-specific recombination system in the yeast S. cerevisiae. Mol. Cell. Biol. *7*, 2087–2096.

Schuldiner, M., Collins, S.R., Thompson, N.J., Denic, V., Bhamidipati, A., Punna, T., Ihmels, J., Andrews, B., Boone, C., Greenblatt, J.F., et al. (2005). Exploration of the function and organization of the yeast early secretory pathway through an epistatic miniarray profile. Cell *123*, 507–519.

Schwartz, B.E., and Ahmad, K. (2006). 2. Chromatin assembly with H3 histones: full throttle down multiple pathways. Curr. Top. Dev. Biol. *74*, 31–55.

Shogren-Knaak, M., Ishii, H., Sun, J.M., Pazin, M.J., Davie, J.R., and Peterson, C.L. (2006). Histone H4–K16 acetylation controls chromatin structure and protein interactions. Science *311*, 844–847.

Smith, J.S., and Boeke, J.D. (1997). An unusual form of transcriptional silencing in yeast ribosomal DNA. Genes Dev. *11*, 241–254.

Smith, J.S., Brachmann, C.B., Pillus, L., and Boeke, J.D. (1998). Distribution of a limited Sir2 protein pool regulates the strength of yeast rDNA silencing and is modulated by Sir4p. Genetics *149*, 1205–1219.

Tsukamoto, Y., Kato, J., and Ikeda, H. (1997). Silencing factors participate in DNA repair and recombination in *S. cerevisiae*. Nature *388*, 900–903.

Utley, R.T., Lacoste, N., Jobin-Robitaille, O., Allard, S., and Cote, J. (2005). Regulation of NuA4 histone acetyltransferase activity in transcription and DNA repair by phosphorylation of histone H4. Mol. Cell. Biol. *25*, 8179–8190.

van Leeuwen, F., Gafken, P.R., and Gottschling, D.E. (2002). Dot1p modulates silencing in yeast by methylation of the nucleosome core. Cell *109*, 745–756.

Winzeler, E.A., Shoemaker, D.D., Astromoff, A., Liang, H., Anderson, K., Andre, B., Bangham, R., Benito, R., Boeke, J.D., Bussey, H., et al. (1999). Functional characterization of the *S. cerevisiae* genome by gene deletion and parallel analysis. Science *285*, 901–906.

Wyce, A., Xiao, T., Whelan, K.A., Kosman, C., Walter, W., Eick, D., Hughes, T.R., Krogan, N.J., Strahl, B.D., and Berger, S.L. (2007). H2B ubiquitylation acts as a barrier to Ctk1 nucleosomal recruitment prior to removal by Ubp8 within a SAGA-related complex. Mol. Cell *27*, 275–288.

Xu, F., Zhang, K., and Grunstein, M. (2005). Acetylation in histone H3 globular domain regulates gene expression in yeast. Cell *121*, 375–385.

Ye, J., Ai, X., Eugeni, E.E., Zhang, L., Carpenter, L.R., Jelinek, M.A., Freitas, M.A., and Parthun, M.R. (2005). Histone H4 lysine 91 acetylation a core domain modification associated with chromatin assembly. Mol. Cell *18*, 123–130.

Yu, C., Palumbo, M.J., Lawrence, C.E., and Morse, R.H. (2006). Contribution of the histone H3 and H4 amino termini to Gcn4p- and Gcn5p-mediated transcription in yeast. J. Biol. Chem. *281*, 9755–9764.

Yuan, D.S., and Irizarry, R.A. (2006). High-resolution spatial normalization for microarrays containing embedded technical replicates. Bioinformatics *22*, 3054–3060.

Yuan, D.S., Pan, X., Ooi, S.-L., Peyser, B.D., Spencer, F.A., Irizarry, R.A., and Boeke, J.D. (2005). Improved microarray methods for profiling the Yeast Knockout strain collection. Nucleic Acids Res. *33*, e103.

Zhou, H., Madden, B.J., Muddiman, D.C., and Zhang, Z. (2006). Chromatin assembly factor 1 interacts with histone H3 methylated at lysine 79 in the processes of epigenetic silencing and DNA repair. Biochemistry *45*, 2852–2861.

Note Added in Proof

The histone mutant libraries described here will be made publicly available by Thermo Fisher/Open Biosystems with the following catalog numbers: YSC5105, Nonessential Histone H3 & H4 Mutant Individual Strain (Yeast); YSC5106, Nonessential Histone H3 & H4 Mutant Collection (Yeast); YSC5135, Histone H3 & H4 Mutant Collection (Bacteria); YSC5136, Histone H3 & H4 Mutant Individual Strain (Bacteria); YSC5138, Essential Histone H3 & H4 Mutant Individual Strain (Yeast); YSC5139, Essential Histone H3 & H4 Mutant Collection (Yeast).

While this paper was under consideration, another collection of histone point mutants was described by Nakanishi et al. (2008; Nat. Struct. Mol. Biol. *15*, 881–888). While many of the data on our two collections are consistent, there are certain mutants defined as lethal in only one of the two studies. Further studies will be necessary to resolve and understand these differences.